JOURNAL OF MATERIALS SCIENCE 27 (1992) 538–552

Synthesis of ceramic membranes

Part II *Modification of alumina thin films: reservoir method*

R. J. R. UHLHORN, V. T. ZASPALIS, K. KEIZER*, A. J. BURGGRAAF
Laboratory of Inorganic Chemistry, Material Science and Catalysis, Faculty of Chemical Engineering, University of Twente, PO Box 217, 7500 AE, Enschede, The Netherlands

Modification of the internal surface of γ-alumina films was realised by an impregnation method employing an aqueous metal salt–urea solution, followed by drying and reaction at 90 °C. Loads of non-supported films were found to be much lower than those of supported films. The support acts as a reservoir, supplying its metal salt under appropriate conditions to the thin film. This results in high loads. A model analysis identified the ratio of the drying time to the reaction time as the critical parameter. With silver, as well as with magnesia, a long reaction time compared to the drying time proved to be favourable. This is best realised by performing the drying (at 40 °C) and the reaction (at 90 °C) sequentially. Silver loads of 70% of the pore volume were realised. A high degree of dispersion upon heating is maintained only under a reducing atmosphere. Up to 85% of the pore volume could be plugged with magnesia. This does not lead to a considerable pore size decrease however, due to the slit shape of the pores.

1. Introduction

The synthesis of γ-alumina thin films with a controllable pore diameter (2.5–10 nm), a sharp pore size distribution and no pinholes or defects has been described before [1]. For use of these membranes in gas separation and catalytically active membrane reactors, it is often necessary to introduce appropriate properties [2]. This can be done by modification of the γ-alumina thin films. The purpose is two-fold. Firstly it is desirable to reduce the pore size in order to enhance gas separation [2]. Secondly, the chemical characteristics of the membrane surface should be controllable, in order to optimize its gas separation and catalytic properties. This article describes a modification method, known as the reservoir method [3], which is especially effective for supported membranes. Application of these membranes in gas separation is described elsewhere [4, 5].

The method is based on the urea method, a well known impregnation technology to deposit a finely dispersed material in a catalyst [6]. The urea decomposes at 90 °C, thereby hydrolysing metal salts present. The hydrolysed metal precipitates. The much larger volume of the support compared to the top layer is employed to create a high load in the top layer only. The support acts as a reservoir, containing material which, under favourable conditions, is precipitated only in the top layer. Two specific species were selected for this type of modification. Magnesium was chosen to enhance the separation of CO_2 [7]. Silver was selected for its catalytic activity in several reactions and its ability to increase hydrogen transport.

First, the experimental procedures are described briefly. Full experimental details and results for the impregnation of non-supported thin films are given. Next the modification of supported thin films will be presented and loads and dispersion compared to those of the non-supported films. This will indicate the increase in effectiveness of the modification due to the presence of the support. A simple model to describe and identify the most important parameters in the reservoir method will be set up. The results obtained with supported thin films concerning load, dispersion and transport properties will be further elaborated in the scope of this model.

2. Experimental procedure

The synthesis of non-supported and supported thin γ-alumina films is described elsewhere [1]. Impregnation solutions of $AgNO_3$–urea and $Mg(NO_3)_2 \cdot 6H_2O$–urea were prepared by dissolving the correct quantities in deionized water while stirring at room temperature. Full details concerning the molarity of the several impregnation solutions are given in the next section.

Non-supported and supported γ-alumina thin films were modified, using a dry impregnation technique. The systems were exposed to the impregnation solution, until saturation had occurred. Then the systems

* Author to whom all correspondence should be addressed.

0022–2461/92 $03.00 + .12

were taken out and the redundant impregnation solutions removed. Full details on the impregnation and subsequent treatments will be given in the next section.

The load of silver or magnesia in non-supported thin films was determined by atomic adsorption spectroscopy (AAS, Perkin Elmer 5000). Transition electron microscopy (TEM) measurements were performed to study the dispersion of silver. In one occasion, X-ray diffraction (XRD) (Philips PW 1370) was employed to study the particle size of silver by X-ray line broadening. N_2 adsorption–desorption measurements, using an ASAP 2400 Micromeritics instrument, were conducted to determine the influence of the deposit on the pore structure.

Modified supported thin films were characterized by gas and water permeability measurements. It was tried to determine the load and profile of the deposit in the support and top layer by energy dispersive X-ray analysis (EDX), using a KEVEX instrument. Scanning auger microscopy (SAM) measurements, using a Perkin Elmer Phi 600 instrument, were performed with the same aim. The effective pore diameter of magnesia modified thin supported films finally was characterized by a cut-off value determination with polyethylene glycol (PEG) [1].

In order to obtain an indication of the reaction kinetics of the deposition of hydrolysed silver and magnesium, solutions of the metal salts and urea were prepared. Five batches of this solution were kept at 90 °C. Each of these batches was successively taken out after about 1 h. The formed precipitate was filtered, dried and weighed. This way the precipitation was followed in time and an estimate of the reaction constant was obtained.

3. Results

3.1. Non-supported thin films

3.1.1. Modification with silver

The decomposition of urea in aqueous media is known to proceed first by an internal reorganization of the urea molecule [4]

$$H_2N\text{–}\underset{\underset{O}{\|}}{C}\text{–}NH_2 \xrightarrow{k_1} NH_4^+CNO^- \qquad (1)$$

while the cyanate ion is rapidly converted to an ammonium ion

$$CNO^- + 2H^+ + 2H_2O \rightarrow NH_4^+ + H_2CO_3 \qquad (2)$$

At room temperature this reaction is complete in the presence of acid only. At 90 °C it is also complete without acid. The rate determining reaction is Reaction 1, which is first order [8]. The reaction constant as a function of temperature is given in Table I.

The silver salt can be hydrolysed according to

$$AgNO_3 + H_2O \rightarrow Ag(OH)\downarrow + H^+ + NO_3^- \qquad (3)$$

and the H^+ must be consumed in the decomposition of urea in order to shift Reaction 3 to the right hand side. Reaction 3 will therefore only proceed if urea decomposition occurs simultaneously. The over-all reaction is

$$2AgNO_3 + CO(NH_2)_2 + 4H_2O \rightarrow 2Ag(OH)\downarrow + 2NH_4NO_3 + H_2CO_3 \qquad (4)$$

Thus one mole of urea is needed per two mole of silver. The kinetics of Reaction 4 were estimated by assuming that this reaction can be described by

$$\frac{d[A]}{dt} = k_n[A]^n \qquad (5)$$

where $[A]$ is the concentration of silver nitrate, k_n the reaction constant and n the order of the reaction. The value of A was determined at a given time in a reaction vessel with a 1.5 M silver nitrate/0.75 M urea solution in water at 90 °C. From this experiment, n was found to be close to one and k_n was found to be 6×10^{-5} s^{-1} at 90 °C. This is only somewhat larger than the reaction rate constant of urea in Table I. Thus the decomposition of urea is presumably the rate determining step.

TABLE I First order rate constants for the decomposition of urea in aqueous solution, after [8]

Temperature (°C)	k_1 (s^{-1}) $\times 10^5$	Medium
70	0.07	Water
80	0.33	Water
90	1.0	Water
95	2.2	Water
100	3.8	Water

Non-supported alumina layers (effective pore diameter 3 nm) were dried in a vacuum furnace at 60 °C for 1 h and then exposed to an aqueous solution of 1.5 M $AgNO_3$ and 0.75 M urea, for 5 min. The impregnated thin films were separated from the impregnation solution by filtering over a Buchner filter and allowed to react at 90 °C for about 3 h by putting the films in a furnace at 90 °C. During this process the thin films are dried simultaneously. This procedure of impregnation, simultaneous drying and reaction was repeated several times. Finally the thin films were heated to 450 °C with a heating rate of 12 °C h^{-1} under a reducing atmosphere (hydrogen gas) to obtain silver precipitates.

At 90 °C the reaction between urea and silver proceeds simultaneously with drying. This drying step will increase the concentration of silver nitrate and urea inside the pores of the γ-alumina film. This can eventually lead to precipitation of these species if the reaction is not complete. It is obvious that the 100 μm thick films are dried quickly at 90 °C. Therefore, presumably, precipitation of the reactants will occur next to reaction. Part of the precipitate will then be a solid state mixture of reactants. This mixture will react further in the calcination step. Probably a small part will melt and dissociate. This occurs below 450 °C [9]. The final product obtained after calcination is silver. Although the composition of the precipitate inside the pores of the γ-alumina films prior to the calcination step is not known, after this heat treatment only silver

was detected. It can be concluded that although ultimately silver is formed, the formation process is very complex due to precipitation and dissociation of various reactants and products. A detailed description of this process is not attempted here.

Table II gives the silver load (determined with AAS) and the dispersion as a function of several variables after calcination. The particle diameters were determined by TEM measurements. The particle size of sample 4 was also determined by XRD line broadening, using a peak fitting program calculating the peak width at half maximum. Table II shows that comparable results are obtained. Fig. 1 presents an example of a TEM picture (for sample 3). At loads up to 17 wt %, the silver is finely dispersed. As more silver is incorporated, the dispersion becomes worse. It is known [10], that silver is very mobile on surfaces, especially at elevated temperatures. In addition to this high mobility, the wettability of silver on γ-alumina is poor. This could be seen on samples 6 and 7, where silver actually formed small droplets on top of the thin films. Therefore silver particles tend to cluster, especially when the temperature, heating rate and the load are high. This explains the poor dispersion of sample 6 and 7.

Table II also demonstrates, that at low loads the calcining atmosphere is not very important. If a slow heating rate is used, the use of hydrogen is not necessary to obtain fine dispersions (sample 4 and 5, Table II). If loads become high, as in supported thin films, hydrogen is absolutely necessary to prevent clustering and sintering of the silver particles. Finally sample 8 in Table II shows that the heating rate is very important, even at low loads. Evidently a high heating rate accelerates clustering and sintering of the silver particles, destroying the dispersion.

To study the influence of the incorporation of silver on the microstructure of the γ-alumina thin films, N_2 adsorption–desorption experiments were performed. Table III gives the results. It can be seen, that the porosity and Brunauer-Emmett-Teller (BET) surface decrease with increasing silver content, but that the pore diameter remains constant. This can be understood with the help of Fig. 2. Here an idealized schematic view of a pore in a γ-alumina thin film is given. The pore has a rectangular shape, with its width much smaller than its length. If a deposit is present in the pore, the pore volume decreases and thus the

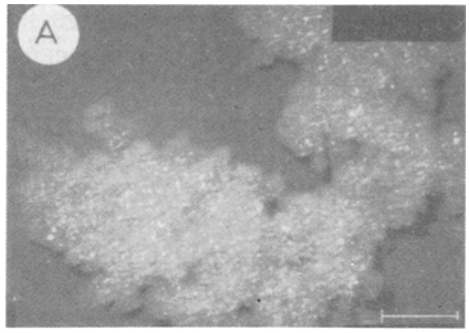

Figure 1 A darkfield TEM picture of a non-supported γ-alumina layer modified with 17 wt % of silver (sample 5, Table II); bar is 100 nm.

TABLE III Structural parameters of non-modified and silver modified thin films, determined from N_2 adsorption–desorption measurements

Sample	Pore diameter (nm)	Porosity (%)	BET surface ($m^2 g^{-1}$)
γ-Al_2O_3	3	51	250
γ-Al_2O_3–Ag	3	48	200

porosity, but not the effective pore width. This could explain the observations of Table III. If the distribution of the deposit is very regular (Fig. 2), an effective decrease in pore width can be expected at a load corresponding to 50% of the pore volume or more. A clustering of the deposit (Fig. 2) on the other hand increases the minimum load for an effective pore size decrease.

It is slightly surprising, that silver particles of 10–20 nm can be incorporated in the γ-alumina pore structure (effective pore diameter 3 nm), without destroying this structure. It must be assumed, that the silver particles are deposited into the length and the depth (plane perpendicular to the paper in Fig. 2) of the pore. It is not likely however, that this is an energetically favourable situation, since restrictions are put upon the particle growth.

3.1.2. Modification with magnesia

The precursor for the modification with magnesium is the magnesium nitrate salt, $Mg(NO_3)_2 \cdot 6H_2O$. This

TABLE II Effect of number of impregnation cycles on the load and dispersion of silver in γ-alumina non-supported thin films

Sample no.	Impregnation cycles	Load % wt[a]	Load Ag/Al_2O_3	Dispersion diameter (nm)	Calcining atmosphere	Heating rate ($°C h^{-1}$)
1	1x	6	0.06	n.d.[b]	H_2	12
2	3x	10	0.11	10	H_2	12
3	4x	13	0.15	10–20[c]	H_2	12
4	4x	11	0.13	10–20	air	12
5	9x	17	0.20	10–20	air	12
6	10x	18	0.21	most > 20	air	12
7	11x	19	0.23	droplets	air	12
8	2x	8	0.09	droplets	H_2	100

[a] = $Ag/(Ag + Al_2O_3)$; [b] = not detectable; [c] = XRD line broadening yielded 17 nm average particle size.

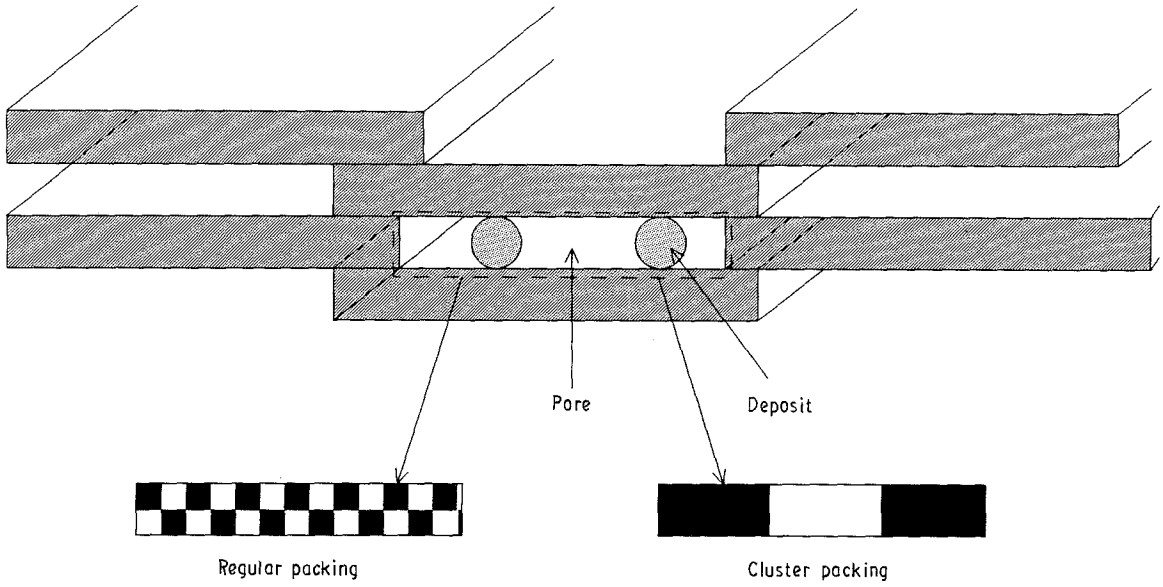

Figure 2 Schematic and idealized representation of a slit-shaped pore in the γ-alumina thin film, containing a deposit (of for example silver).

salt dissolves and dissociates readily in water [9]. It can be hydrolysed according to

$$Mg(H_2O)_6^{2+} \rightarrow Mg(OH)_2 \downarrow + 4H_2O + 2H^+ \quad (6)$$

and the H^+ is consumed in the decomposition of urea (Reactions 1 and 2). Reaction 6 will therefore only proceed if urea decomposition occurs simultaneously. The over-all reaction can be written as

$$Mg(H_2O)_6^{2+} + 2NO_3^- + CO(NH_2)_2 \rightarrow$$

$$Mg(OH)_2 \downarrow + 2NH_4NO_3 + H_2CO_3 + 2H_2O \quad (7)$$

Thus one mole of urea is needed per one mole magnesium. In analogy to the silver Reaction 3 the kinetics of Reaction 7 was estimated. For this purpose the increase in magnesium hydroxide precipitate was followed in time in a reaction vessel, containing a 1 M $Mg(NO_3)_2$/2 M urea solution in water. With the help of Equation 5 and Reaction 7, an order of reaction and reaction constant could be determined. Due to the slow reaction, an estimation of the order of reaction was very inaccurate. A reaction constant in the order of 4×10^{-6} s^{-1} was estimated. Although this absolute value is disputable, it can still be concluded that the precipitation in Reaction 6 is slower than the urea decomposition reaction. Therefore the rate determining step in the magnesium modification is the precipitation reaction, in contrast with the silver modification process.

Non-supported γ-alumina thin films with effective pore diameter of 3 nm were dried at 60 °C in a vacuum oven and then exposed to a 1 M magnesium salt–2 M urea solution in water for 5 min. The impregnated thin films were separated from the impregnation solution by filtering over a Buchner filter and allowed to react at 90 °C for about 4 h by putting the films in a furnace. This procedure was repeated several times. Finally the thin films were heated to 380 °C with a heating rate of 12 °C h^{-1}. In this heating step magnesium oxide is formed. Since the mobility of magnesia is negligible, no special calcining atmosphere was necessary.

TABLE IV Effect of number of impregnation cycles on the load of magnesia in γ-alumina non-supported thin films, using a 1 M $Mg(NO_3)_2$–2 M urea solution

Impregnation cycles	Load	
	% wt[a]	Mg/Al_2O_3
4x	1.0	0.010
5x	1.7	0.017
6x	1.9	0.019
8x	2.0	0.020
10x	2.3	0.023
11x	2.4	0.025

[a] = $MgO/(MgO + Al_2O_3)$.

Reaction 7 between magnesium and urea is slower than the corresponding reaction between silver and urea. Simultaneous drying and reaction will almost certainly lead to precipitation of a part of the reactants. This mixture will react further in the calcination step. Probably a small part will melt and dissociate. This occurs below 350 °C [9]. The final product obtained after calcination is magnesia. In analogy with silver it can be concluded that the formation of magnesia is very complex due to precipitation and dissociation of various reactants and products, occurring simultaneously with Reaction 7. A detailed description of the process is not attempted here.

Table IV gives the load, as determined by AAS. The loads are very low. For this reason, no dispersion analysis was performed. In N_2 adsorption–desorption experiments no difference could be detected between the non-modified and modified thin films. Obviously the loads are too low to influence the microstructure of the thin film.

3.2. Supported thin films

3.2.1. Modification with silver

Supported thin films, consisting of an α-alumina support, pore diameter 0.13 μm, porosity 45%, thickness

2 mm and cross section 39 mm and a 5 μm thick γ-alumina film with effective pore diameter of 3 nm, were impregnated with silver–urea solutions of varying concentrations. The supported thin films were exposed to the solution for 30 min. After removal of the redundant solution, they were put on a non-porous plate, with the top layer facing upwards. This way drying occurs mainly through the top layer. The system was dried for 3 h at 40 °C and 60% relative humidity and then heated to 90 °C. It was kept at this temperature for another 3 h. In one occasion the system was directly heated to 90 °C and kept at this temperature for 3 h. The reacted system was heated from room temperature at a rate of 12 °C h^{-1} to 450 °C under hydrogen. In this heat treatment silver is formed. The heat treatment was based on the results with non-supported films, where the heating rate proved to be especially important.

The load of silver in the system was determined by AAS and by calculation from the concentrations of the impregnation solution. Both methods yield the same result, as indicated in Table V. From this table and Table II it is clear, that much higher loads are possible in supported films than in non-supported films. The initial concentration and the procedure followed determine the final load. It is not possible to incorporate more than 67 wt % silver (corresponding to 70% of the pore volume) and keep the silver inside the thin supported film.

The much higher loads can be qualitatively understood with the help of Fig. 3. The pore volume of the support is much larger than the pore volume of the top layer. Upon drying capillary forces are developed in the support as well as the top layer. Since the pore size in the top layer is much smaller, the capillary forces are much larger here. Thus a (capillary) pressure drop is created inside the system, causing the flow of liquid from the support to the top layer. The support acts as a reservoir, supplying impregnation solution to the top layer. The concentration of silver reactant in the top layer will increase, resulting in high silver loads of the top layer. A model to identify the most important parameters in the reservoir method is presented in the next section.

Characterization of the dispersion of silver in supported films is much more difficult than in non-supported films. TEM and XRD measurements are no longer possible, due to the presence of the support. In order to obtain an indication of where the silver is deposited, a cross-section of the support–top layer system was analysed by EDX. Fig. 4 presents such an EDX scan. The white line presents the silver content. In this case most of the silver is present in the top layer. Table V shows that this is also true for all the other samples, except one. The top layer of the sample, that is directly heated to 90 °C, contains hardly any silver. In this sample, drying and reaction (at 90 °C) occur simultaneously, while in the other samples drying and reaction occur sequentially (at 40 °C no reaction takes place). In the first case most of the silver is deposited in the support, while in the second case most of the silver is present in the top layer. This difference is explained later in combination with the model presented in the next section.

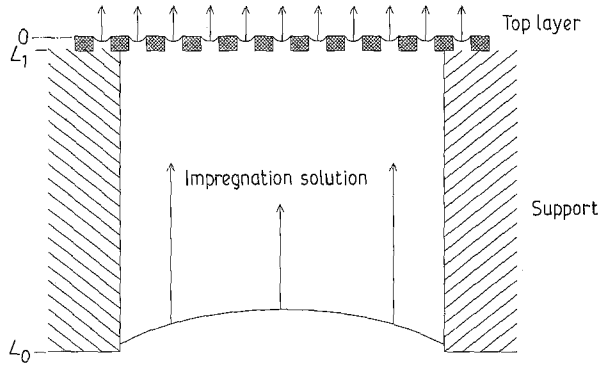

Figure 3 Schematic and idealized representation of a support pore and top layer pores, filled with impregnation solution.

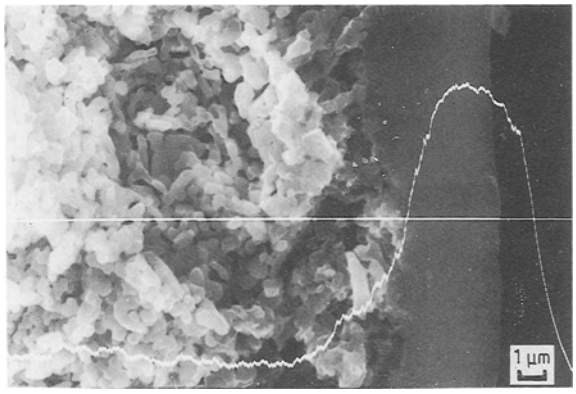

Figure 4 EDX scan on a top layer–support cross-section. The white line represents the amount of silver, which is mainly present in the top layer.

TABLE V Silver loads as a function of impregnation solution concentration and reaction–drying procedure for a supported thin γ-alumina film, calcined at 450 °C

Sample	Load		AAS load % wt[a]	$AgNO_3$ ($g l^{-1}$)	Urea ($g ml^{-1}$)	Drying + reaction
	% wt[a]	% vol[b]				
1	7.5	2.8	7.5	1.28	0.228	sequential
2	10.0	3.9	10	1.93	0.343	sequential
3	15	6.2	15	3.07	0.545	sequential
4	50	35.0	50	14.48	2.58	sequential
5	67	71.5	67	92.64	16.45	sequential
6	15	6.2	–	3.07	0.545	simultaneous

[a] = $Ag/(Ag + Al_2O_3)$; [b] = percentage of the initial pore volume of the top layer.

To gain more insight into the dispersion of silver in the top layer, samples 4 and 6 in Table V were subjected to a SAM measurements. A compositional analysis on several points in the cross-section of the top layer was performed. Although SAM is well-understood in characterization of dense surfaces [11, 12], it is not well-understood yet when applied on porous surfaces. A second problem is the insulating character of the alumina system. This hampers analysis. These two aspects, the porosity and the insulating character, make a reliable quantitative analysis impossible. Fig. 5, presenting the silver composition profile in two cases, should therefore only be interpreted in a qualitative sense.

If drying and reaction occur simultaneously (sample 6, Fig. 5), a substantial amount of silver is found in the support. The silver found in the top layer, is distributed homogeneously (Fig. 5). The other sample shows a totally different picture. Here all the silver is collected in the first 0.5 μm of the top layer, near the pore entrance. The support does not contain any silver. Table V already showed, that the top layer of the sample prepared by simultaneous drying and reaction (at 90 °C, sample 6) contains hardly any silver. This is verified by the SAM results, where most of the silver present is found in the support. This result is explained later in combination with the model presented in the next section.

To determine the effect of the silver incorporation in the top layer microstructure, gas permeation measurements were performed. Fig. 6 presents a representative gas permeability plot for a non-modified and modified supported thin film. It shows that before, as well as after, modification the transport of helium through the top layer can be described by Knudsen diffusion [7]. The introduction of large amounts of silver in the top layer obviously does not cause defects or pinholes. This is slightly surprising, considering the small pore diameter of the γ-alumina (3 nm). The load of 67 wt % means that about 70% of the pore volume is occupied by the silver (Table V). However, it should be remembered that the pores in the γ-alumina are slit-shaped. Fig. 2 shows, that the slit shaped pores are only small in one dimension and not in the other two. Therefore a large amount of silver could be introduced, without destroying the structure. Fig. 2 also

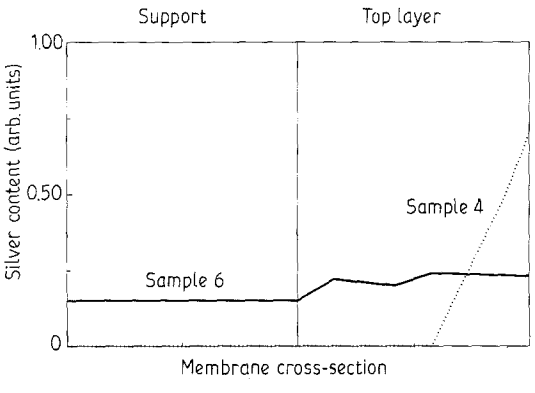

Figure 5 SAM point analysis of supported (Ag modified) γ-Al_2O_3 cross-section of samples 4 and 6 in Table V.

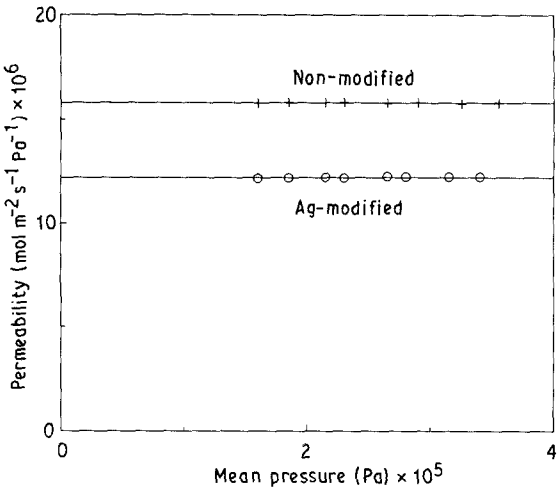

Figure 6 Helium gas permeability data for a (+) non-modified and (○) silver modified supported thin film of 5 μm thickness, data were corrected for the influence of the support.

demonstrates, that the silver does not cause a pore size decrease, but only a decrease in pore volume. This pore volume decrease causes the decrease in permeability. According to the experimental results more than 70% of the pore volume should be filled in order to obtain a pore size decrease (Table V). This means the silver is not deposited regularly, but more in clusters (Fig. 2). Since the length of the pore is at least ten times the width (at least 30 nm [1]), a high percentage of the pore volume should be filled by deposit, to obtain an effective pore size decrease. Introducing these large amounts of silver is not possible, because at these high loads silver introduces defects in the top layer.

3.2.2. Modification with magnesia

Supported thin films of identical dimensions as in the previous section were impregnated with $Mg(NO_3)_2$–urea solutions of varying concentrations. The supported thin films were exposed to the solution for 30 min. After removal of the redundant solution, they were put on a non-porous plate, with the top layer facing upwards. This way drying occurs mainly through the top layer. The system was either dried for 3 h at 40 °C and 60% relative humidity and then heated to 90 °C and kept at this temperature for another 3 h or directly heated to 90 °C and kept at this temperature for 3 h. Heat treatment occurred at 380 °C (rate 12 °C h^{-1}) for 3 h. After the heat treatment, the impregnation process was repeated. In one occasion the load of magnesia in the support and top layer was determined by AAS. The result was in correspondence with the load calculated from the volume of the system and the concentration of the impregnation solution. Therefore all the succeeding loads were calculated in this way.

Table VI summarizes the several procedures and the loads they yield. These are mean values of at least two separate experiments. Samples 1–3 were prepared by heating the impregnated supported films immediately to 90 °C. Thus drying and reaction occurred simultaneously in those samples. Samples 4–6 were

TABLE VI Magnesia loads and permeability as a function of impregnation solution concentration and reaction–drying procedure for a supported thin γ-alumina film, calcined at 380 °C

Sample	Solution $Mg(NO_3)_2$:urea (M)	Cycle	Load		F_0^G [c] (mol m^{-2} s^{-1} Pa^{-1}) ($\times 10^{-6}$)	Drying + reaction
			% wt[a]	% vol[b]		
1	0.05:0.1	1x	30	44	8.9 (26%)[d]	simultaneous
2	0.05:0.1	2x	40	69	5.8 (52%)[d]	simultaneous
3	0.05:0.1	3x	45	85	5.4 (55%)[d]	simultaneous
4	0.12:0.24	1x	30	44	9.8 (24%)[e]	sequential
5	0.12:0.24	2x	40	69	6.1 (53%)[e]	sequential
6	0.12:0.24	3x	45	85	1.3 (90%)[e]	sequential

[a] = $MgO/(MgO + Al_2O_3)$; [b] = percentage of the initial pore volume of the top layer; [c] = helium gas permeability; [d] = non-modified 12.1×10^{-6} mol m^{-2} s^{-1} Pa^{-1}; [e] = non-modified 12.8×10^{-6} mol m^{-2} s^{-1} Pa^{-1}.

prepared by first drying and then heating to 90 °C. Thus drying and reaction were performed sequentially in those samples. In analogy with the silver high loads of magnesia are obtained due to the support, which acts as a reservoir.

After reaction, the pore is presumably filled with $Mg(OH)_2$ (Reaction 7). As discussed before it is possible that part of the precipitate consists of a solid state mixture of reactants ($Mg(NO_3)_2$/urea), due to saturation of the impregnation liquid in the top layer. Since this cannot be quantified it is assumed that the precipitate is $Mg(OH)_2$ only. It can be calculated, that the 0.05 M $Mg(NO_3)_2$/0.10 M urea impregnation solution inside the support yields precisely enough $Mg(OH)_2$ to fill the 5 μm thick top layer completely. The density of $Mg(OH)_2$ was taken to be 2.36 g cm^{-3} [9]. Upon calcination, magnesia is formed with a much higher density (3.58 g cm^{-3} [9]). This is accompanied by shrinkage and consequently the pores open again. Only part of the pore volume is occupied by magnesia (Table VI). The impregnation cycle is repeated, but now only part of the initially available pore volume can be occupied by $Mg(OH)_2$, since some magnesia is already present. If it is assumed, that all the remaining pore volume is occupied by $Mg(OH)_2$, which forms magnesia after heat treatment, the pore volume totally occupied by magnesia after the second (and third) impregnation cycle can be calculated. These numbers are also presented in Table VI. Since 0.05 M $Mg(NO_3)_2$ supplies the maximum load (top layer is completely filled), there is no difference in theoretical load if the concentration of the impregnation solution is increased to 0.12 M $Mg(NO_3)_2$ (Table VI). In this latter case magnesia is also precipitated in the support.

To determine the load in the top layer only, a cross-section of the support–top layer system of sample 2 was analysed by EDX. Photographs identical to Fig. 4 were obtained, only this time the line represented magnesia. The magnesia was only present in the top layer. Note that in the case of sample 2, drying and reaction occurred simultaneously at 90 °C. Still, all the magnesia is present in the top layer, contrary to the results with silver. Consequently there must be a difference between the silver and magnesium modification, likely due to the difference in reaction time. This is also elucidated after the presentation of the model in the next section.

To get a more detailed picture of the dispersion, a SAM analysis was conducted on the same cross-section. This proved to be very difficult however, due to low sensitivity of magnesium compared to aluminium. Results were very difficult to obtain and not reliable. Therefore the dispersion of magnesia inside the top layer is not known accurately.

To study the influence of the incorporation of magnesia on the microstructure of the γ-alumina thin film, gas permeability measurements were performed and tabulated in Table VI. No gas permeability could be detected after heat treatment at 90 °C, but prior to calcination. The top layer is completely blocked by $Mg(OH)_2$. After heat treatment the helium gas permeability is, in all cases, no function of pressure and Knudsen diffusion is the dominant transport mechanism. It can be concluded, that incorporation of magnesia does not lead to the introduction of cracks or large pinholes.

Table VI shows there is no difference between samples 1–4 and between samples 2–5. This means that in the case of magnesia there is no difference between performing the drying and reaction simultaneously or sequentially. This can be explained with the model in the next section. There is however a large difference between samples 3 and 6. Performing drying and reaction simultaneously seems to give rise to a maximum decrease in permeability, while performing reaction and drying sequentially does not so.

A last problem to address is whether or not the high loads of magnesia lead to a pore size decrease. In the previous section it was stated that more than 70% of the pore volume should be filled to decrease the (slit-shaped) pore size effectively. A cut-off value determination, performed on sample 4 and shown in Fig. 7, showed this to be true. After the first impregnation cycle (decrease in pore volume 44%) no change in cut-off value was detected, indicating a constant pore size. Again in this case only the pore volume is decreased.

Unfortunately this kind of experiment is not possible with samples 5 and 6, due to the resulting very low water flux. In Section 5 it will be shown, that only a very small pore size decrease is obtained. Apparently at least 85% of the pore volume should be filled to decrease the pore size effectively. This supports the cluster like distribution of the deposit in the pore (Fig. 2). Since this will also result in a sharp decrease of permeability, *in situ* modification does not seem very suitable to diminish the pore size of γ-alumina films. It

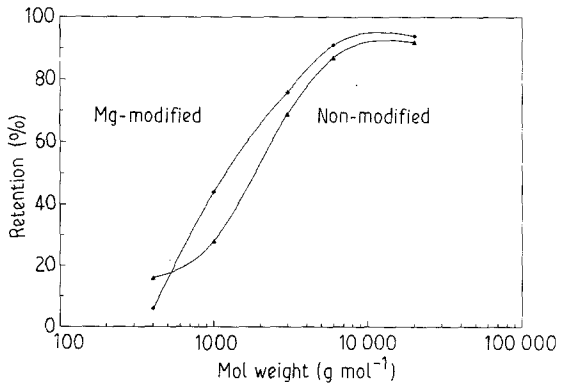

Figure 7 Retention values as a function of molecular weight for PEG, (▲) before and (■) after modification with magnesia.

is however very suitable to change and control the chemical characteristics of the membrane surface. An alternative method to decrease the pore size has been developed [5].

4. Modelling of the reservoir method

4.1. Drying and reaction of the support and top layer

4.1.1. General set-up

This section is meant to analyse the most important parameters in the reservoir method with a simple model and to give the lines, along which a more sophisticated model can be set up.

The starting situation is given in Fig. 3. The pores of the support are completely filled with impregnation solution, as are the pores of the top layer. It is assumed here, that the impregnation solution consists of reactant A (the metal salt) and C (the urea). Reactant A can be converted to product B (the metal hydroxide), according to

$$A \rightarrow B\downarrow \tag{8}$$

where it is assumed that B is deposited as soon as it is formed. The reaction of Equation 8 is assumed to be rate determining. It is also assumed that the reactants are infinitely soluble. No precipitation of reactants due to saturation will occur. The system support top layer (Fig. 8) is dried through the pores of the top layer only. This drying can be divided into two steps: the drying of the support (this section) and the drying of the top layer only (next section). For convenience it is assumed that the drying of the support starts at time $t = 0$ and ends at time $t = t_1$. The volume of impregnation solution in the top layer is constant in this time interval. The volume of the impregnation solution in the support decreases due to removal of water vapour from the top layer. Drying of the top layer starts at a time $t = t_1$ and now the liquid volume accomodated in the top layer will decrease.

The following assumptions are made:

1. The diffusion of species in the solution is assumed to be much faster than the drying and reaction rates. Therefore no (salt) concentration gradients exist inside the pores of the support or the pores of the top layer. In fact the support pore and the top layer pore are considered to be two continuously ideally stirred tank reactors in series.
2. The drying conditions do not change during the process of drying the support. This means the temperature, pressure and relative humidity are assumed to be constant, as well as the surface area available for drying.
3. Reactants A and C are infinite soluble, while product B is non-soluble.
4. The reaction of reactant A to product B is con-

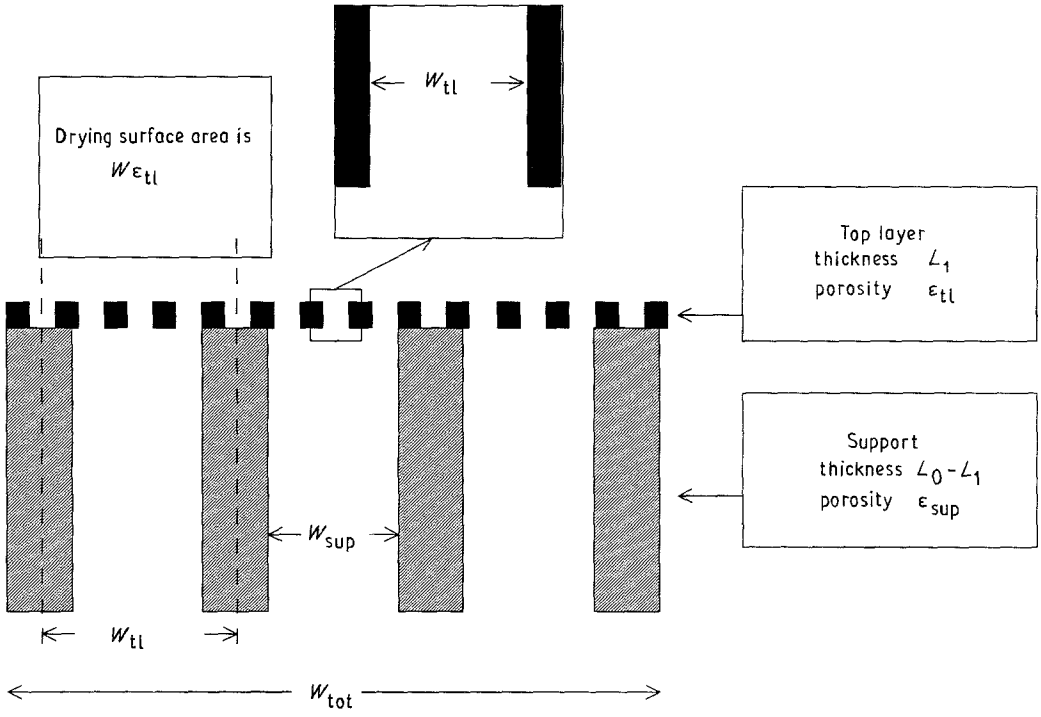

Figure 8 Schematic and idealized representation of support and top layer pores, filled with impregnation solution, and some important parameters of the reservoir model; note that $W_{sup} = W^*\varepsilon_{sup}$.

sidered to be first order. The product B is immediately deposited after reaction.
5. The volume of the top layer pores is assumed to be constant.
6. The pore size distributions of support and top layer are considered uniform.
With these assumptions, an analysis can be made.

4.1.2. Profiles in the support at time $t \leqslant t_1$

The amount of product B, deposited inside the support pore can be calculated by

$$M_{B,sup}(t) = M_{A,sup,0} - M_{A,sup}(t) - M_{A,trans}(t) \quad (9)$$

where $M_{B,sup}(t)$ is the amount of B deposited at time t (mol), $M_{A,sup,0}$ the amount of A initially present in the support, $M_{A,sup}(t)$ the amount of A present in the support pore at time t and $M_{A,trans}(t)$ the amount of A transported to the top layer at time t. The right hand side of Equation 9 expresses the amount of A that has reacted and thus the amount of B formed. The amount of A present and the amount of A transported are dependent upon the reaction and drying rates. An analysis of these processes is therefore appropriate.

The volume change of the liquid due to drying can be described by Fig. 8

$$V_{sup}(t) = V_{0,sup} - aW_{sup}(\varepsilon_{tl}/\varepsilon_{sup})t \quad (10)$$

where $V_{sup}(t)$ is the impregnation solution volume in the support pore after time t, $V_{0,sup}$ is the initial support pore volume, a is a drying constant ($m\,s^{-1}$), which is only dependent on the drying conditions (temperature, pressure, relative humidity). The drying surface area per support pore is given by $W_{sup}(\varepsilon_{tl}/\varepsilon_{sup})$ (Fig. 8), where ε_{tl} and ε_{sup} are the porosities of the top layer and support, respectively, and W_{sup} the cross-section of the support pore. This can be understood considering the drying surface area is made up of all the (interconnected) pores of the top layer. Finally t represents the drying time. It is possible to formulate a characteristic drying time of the support

$$\tau_{sup} = \frac{(L_0 - L_1)}{a(\varepsilon_{tl}/\varepsilon_{sup})} \quad (11)$$

where $(L_0 - L_1)$ represents the length of the support pore (Fig. 3). This will prove to be an important parameter.

The reaction, which is assumed to be first order, can be described by

$$\frac{d[A]_{sup}(t)}{dt} = -K_1[A]_{sup}(t) \quad (12)$$

with $[A]_{sup}(t)$ the concentration of A in the support ($mol\,m^{-3}$) and K_1 the reaction constant (s^{-1}). Equation 12 is equal to Equation 5 with $n = 1$. A characteristic time of reaction is given by

$$\tau_{re} = 1/k_1 \quad (13)$$

The amount of A, which reacts between time $t = 0$ and time $t = t_1$, can be derived from Equation 12. Assume that

$$C_A = \frac{[A]}{[A]_0} \quad C_A \in [0, 1]$$
$$\tau = \frac{t}{\frac{(L_0 - L_1)}{a(\varepsilon_{tl}/\varepsilon_{sup})}} \quad \tau \in [0, 1] \quad (14)$$

where $[A]_0$ is the initial concentration of A. By the introduction of Equation 14 in Equation 12 this equation becomes dimensionless

$$\frac{dC_{A,sup}(\tau)}{d\tau} = -\frac{k_1(L_0 - L_1)}{a(\varepsilon_{tl}/\varepsilon_{sup})} C_{A,sup}(\tau) \quad (15)$$

with $C_{A,sup}(\tau)$ the dimensionless concentration of A in the support. The right hand side of Equation 15 can be rewritten as

$$\frac{K_1(L_0 - L_1)}{a(\varepsilon_{tl}/\varepsilon_{sup})} = \frac{(L_0 - L_1)/a(\varepsilon_{tl}/\varepsilon_{sup})}{1/K_1} = \frac{\tau_{sup}}{\tau_{re}} \equiv \varphi \quad (16)$$

Thus the parameter φ represents the ratio of the characteristic time of drying to the characteristic time of reaction. If the drying is fast compared to the reaction, φ is small. If the reaction is fast compared to the drying, φ will be large. Substitution of Equation 16 in Equation 15 and solving this equation with the boundary condition that $C_A = 1$ at $\tau = 0$ gives the simple solution

$$C_{A,sup}(\tau) = e^{-\varphi\tau} \quad (17)$$

Equation 17 presents the change in the dimensionless concentration of A in the support. It shows that the concentration of reactant A in the support decreases only due to reaction since the volume decrease due to drying does not influence the concentration. Equation 17 also shows that at high φ (fast reaction compared to drying), A reacts mainly in the support. Thus a high reaction rate in comparison to the drying rate will lead to a reaction of A predominantly in the support.

Although the concentration of reactant A only changes due to reaction (Equation 7), the total amount of reactant A present at any time in the support pore (M_A) also changes due to transport of A to the top layer in order to refill the evaporated volume. The amount present at time τ in the support is equal to

$$M_{A,sup}(\tau) = C_{A,sup}(\tau)[A]_0 V_{sup}(\tau) = C_{A,sup}(1 - \tau)M_{A,0,sup} \quad (18)$$

since $V_{sup}(\tau)$ can be described by combining Equations 10 and 14

$$V_{sup}(\tau) = V_{0,sup}(1 - \tau) \quad (19)$$

The dimensionless amount of A present as a function of τ and φ is given by

$$N_{A,sup}(\tau) = \frac{M_{A,sup}(\tau)}{M_{A,0,sup}} = (1 - \tau)C_{A,sup}(\tau) = (1 - \tau)e^{-\varphi\tau} \quad (20)$$

Comparison of Equations 17 and 20 show, that the dimensionless amount of A present in the support decreases faster than the dimensionless concentration of A in the support, due to the extra factor $(1 - \tau)$ in Equation 20. This faster decay of the amount of A present is due to transport of A from the support to the top layer. If φ is high (fast reaction), the effect is less pronounced, since most of the A present will react quickly to give B.

The cumulative amount of A transported to the top layer in a time t, $M_{A,\text{trans}}$, is given by the sum of drying volume times the concentration of A in the support pore in a small time dt

$$M_{A,\text{trans}}(t) = \int_0^t a(\varepsilon_{tl}/\varepsilon_{sup}) W_{sup}[A]dt \quad (21)$$

and by substitution of Equation 14 and rearrangement

$$M_{A,\text{trans}}(\tau) = \int_0^\tau C_{A,sup}(\tau) M_{A,0,sup} dt \quad (22)$$

Solving Equation 22 and expressing the amount transported in dimensionless form yields

$$N_{A,\text{trans}}(\tau) = \frac{M_{A,\text{trans}}(\tau)}{M_{A,0,sup}} = \frac{1}{\varphi}(1 - e^{-\varphi\tau}) \quad (23)$$

Fig. 9 gives the dimensionless amount of A transported to the top layer as a function of φ and τ. If the drying rate is much higher than the reaction rate (small φ), most of the A is transported, as is demonstrated in Fig. 9. The opposite case, a low drying rate compared to the reaction rate (high φ), results in almost no transport of A. This is because most of A will react in the support to give B (see also Equations 17 and 20).

Now the amount of B formed inside the support pore can be calculated according to Equation 9. Combining this equation with Equation 18 and Equation 23 gives

$$N_{B,sup}(\tau) = \frac{M_{B,sup}(\tau)}{M_{A,0,sup}} = 1 - e^{-\varphi\tau}(1 - \tau) - \frac{1}{\varphi}(1 - e^{-\varphi\tau}) \quad (24)$$

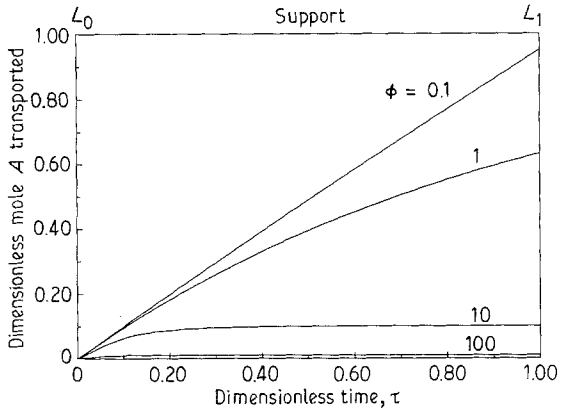

Figure 9 Dimensionless amount of mole A transported to the top layer as a function of the dimensionless time, τ, for several φ.

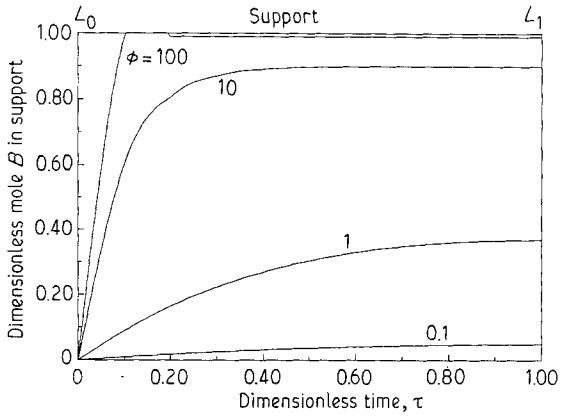

Figure 10 Dimensionless mole of product B deposited in the support as a function of the dimensionless time, τ, for several φ.

with $N_{B,sup}(\tau)$ the dimensionless amount of B deposited in the support pore. Fig. 10 presents the dimensionless deposit of B as a function of τ and φ. At small φ (drying fast) almost no B is deposited and almost all A is transported (Figs 9 and 10). At high φ (reaction fast) almost all B is deposited and almost no A is transported (Figs 9 and 10).

4.1.3. Profiles in the top layer at time $t \leqslant t_1$

During drying of the support, the volume of the top layer is assumed to be constant. This implies, that the volume changes by deposition of B in the top layer pore are assumed to be negligible compared to the total volume. Obviously this assumption will fail at high loads. The model described below is therefore only valid at low loads. The qualitative influence of high loads on the deposition profile will be presented in the next section.

The concentration of A in the top layer will change by reaction and by supply from the support. Since the volume in the top layer pore is constant, the amount of A is also only changed by reaction and supply from the top layer.

The total supply of A from the support per unit time is given by

$$M^*_{A,\text{trans}}(t) = a(\varepsilon_{tl}/\varepsilon_{sup}) W_{sup}[A]_{sup}(t) \quad (25)$$

according to Equation 21. This is distributed over all the pores of the top layer however. The ratio, R, of the total number of pores in the top layer to the total number of pores in the support is given by

$$R = \frac{W_{sup}\varepsilon_{tl}}{W_{tl}\varepsilon_{sup}} \quad (26)$$

with W_{tl} the cross-section of a top layer pore. This can be understood, assuming straight cylindrical pores. The total amount of pores in the top layer is given by $\varepsilon_{tl} W_{tot}/W_{tl}$ (Fig. 8), where W_{tot} is the total surface area. The total amount of reactant A supplied per unit time per pore of the support to one pore in the top layer is given by the ratio $M^*_{A,\text{trans}}(t)/R$. A mass balance over A in the pore of the top layer now yields

$$\frac{dM_{A,tl}(t)}{dt} = -K_1[A]_{tl}(t) + aW_{tl}[A]_{sup}(t) \quad (27)$$

where $M_{A,tl}$ is the total amount of A present in the top layer pore. This equation is dimensionalized in analogy with Equation 14 and rearranged to give

$$\frac{dC_{A,tl}(\tau)}{d\tau} = -\varphi C_{A,tl}(\tau) + \underbrace{\frac{(L_0 - L_1)}{L_1}(\varepsilon_{sup}/\varepsilon_{tl})}_{Q} C_{A,sup}(\tau) \quad (28)$$

The term (Q) can be understood by rewriting this term in the form

$$\frac{(L_0 - L_1)}{L_1}(\varepsilon_{sup}/\varepsilon_{tl}) = \frac{(L_0 - L_1)}{a(\varepsilon_{tl}/\varepsilon_{sup})} \Big/ \frac{L_1}{a} \equiv Q \quad (29)$$

Q represents the ratio of the characteristic drying time in the support and the characteristic drying time in the top layer. The concentration of A relative to the initial concentration of A in the top layer pore is given by

$$C_{A,tl}(\tau) = \int_0^\tau \{-\varphi C_{A,tl}(\tau) + QC_{A,sup}(\tau)\} d\tau \quad (30)$$

where $C_{A,sup}(\tau)$ is given by Equation 17. Fig. 11 presents the dimensionless concentration of A within the top layer as a function of time τ. This was generated by numerically solving Equation 30. If the drying rate is high (small φ), there is a large concentration increase. If the reaction rate becomes higher with respect to the drying rate, less A will be introduced. The concentration of A in the top layer will still increase however. This also increases the amount reacted. It is possible, that after a certain time the reaction consumes more A than is supplied by the support. Thus initially the concentration of A increases (supply larger than reaction), the amount reacted increases and this leads to a decrease in the concentration of A (reaction faster than supply). This explains the maximum as observed in Fig. 11 for $\varphi = 10$. With large drying rates (low φ), the dimensionless concentration of A can become very high (Fig. 11). So it is shown, that drying of the support through the top layer can result in accumulation of A in the top layer.

The profile of B in the top layer is much more simple to derive. Since it is assumed, that no B is transported from the support, B is only generated by reaction in the top layer pore. This results in

$$\frac{d[B]_{tl}(t)}{dt} = K_1[A]_{tl}(t) \quad (31)$$

Dimensionalization and rearranging results in

$$C_{B,tl}(\tau) = \int_0^\tau \varphi C_{A,tl}(\tau) d\tau \quad (32)$$

where $C_{B,tl}$ is the dimensionless concentration of B in the top layer. Fig. 12 presents $C_{B,tl}$ as a function of τ and φ. This was generated by numerically solving Equation 32. At high drying rates, the concentration of A in the top layer is high, but the reaction rate is low. Therefore the concentration of B is not too high. With increasing reaction rate, the concentration of A in the top layer pore is lowered, but more A reacts. This results in first an increase in concentration of B and then a decrease (Fig. 12). This is even better demonstrated in Fig. 13. Here the dimensionless amount of B is plotted as a function of φ. Fig. 13 clearly shows that the dimensionless amount of B passes through a maximum, as was predicted from Fig. 12. It should be noted, that the dimensionless amount of B at the maximum φ is very high. Thus Figs 11–13 show, that the support can act as a reservoir, leading to high loads of A and B in the top layer.

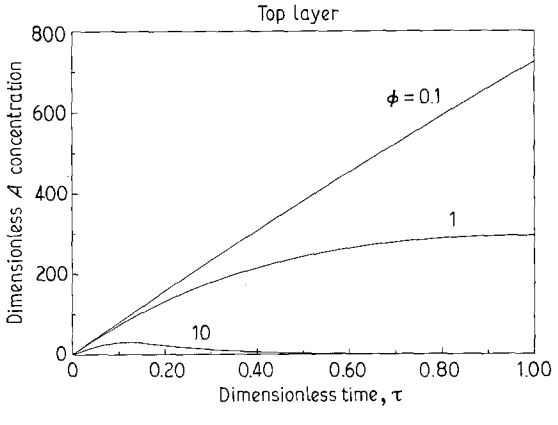

Figure 11 Dimensionless concentration of reactant A present in the top layer as a function of the dimensionless time, τ, for several φ.

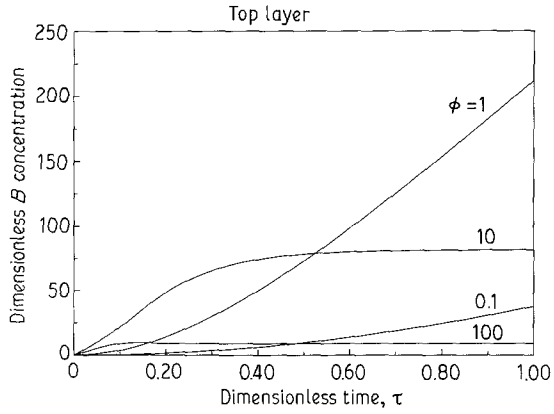

Figure 12 Dimensionless concentration of B deposited in the top layer, upon drying of the support, as a function of the dimensionless time, τ, for several φ.

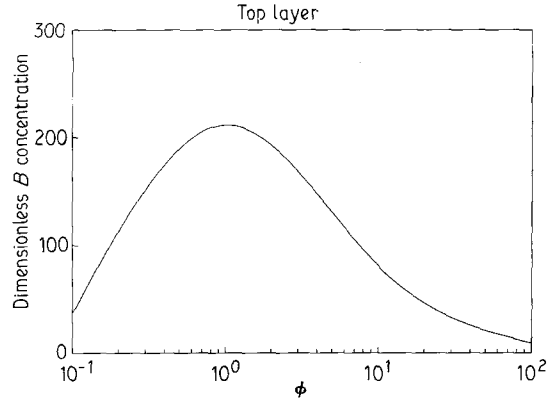

Figure 13 Dimensionless amount of B deposited in the top layer upon drying of the support as a function of the parameter φ at $\tau = 1$ (support completely dried).

4.1.4. Summary

In the previous section the influence of drying of the support, containing impregnation liquid, upon the concentration of reactant A and product B in the top layer, has been analysed. The most important parameter in the process is φ, which represents the ratio of the characteristic times of drying to the reaction. If the reaction is fast compared to the drying rate (high φ), most of reactant A is converted to B inside the support. In the top layer no enrichment of A or deposition of B occurs. The opposite case, a high drying rate compared to the reaction rate (low φ), results in a large increase in the concentration of A in the top layer up to 750 times the initial concentration. The deposition of B as a function of φ goes through a maximum however, since at low φ, the reaction rate in the top layer is also low. Still at low φ, a substantial deposition of B inside the top layer can be expected. Since the whole top layer pore is continuously filled with (ideally stirred) liquid, the deposition will be homogeneously divided over the top layer.

4.2. Drying and reaction in the top layer: $t \geqslant t_1$

4.2.1. General set-up

The next stage in the reservoir method to be described, is the drying of the top layer only. This stage is entered after the support is completely dry. It is expected to give rise to a thickness profile of B inside the top layer pore.

This second stage is much more difficult to describe, since several effects occur at the same time. Consider a top layer pore filled with impregnation liquid (Fig. 14). The following processes occur

1. The volume of impregnation liquid decreases due to drying (Fig. 14).
2. The volume of the top layer pore changes due to deposition of product B; this in turn will influence the drying surface area and thus the drying rate.

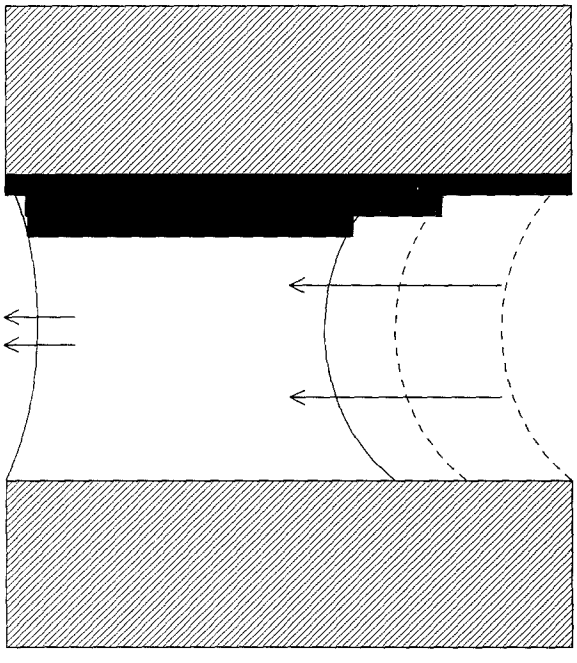

Figure 14 Deposition profile of product B in a top layer pore which is dried from the top.

A complete analysis of this problem must include a pore geometry model, in order to account for the change in drying surface due to the deposition. An additional complicating factor is that the drying time is low, due to the small pore volume. Therefore it is likely that in this case precipitation of reactants will also occur, especially at high reactant concentrations. This is considered to be outside the scope of this model. Therefore a very simple model will describe the possible profiles. The change of drying surface and precipitation of reactants will be introduced as disturbance factors. The qualitative consequences of these disturbance factors are given.

4.2.2. Profiles upon drying and reaction in the top layer

Fig. 14 pictures the starting situation. The top layer pore is completely filled with impregnation solution and is dried from one side. For the moment, the drying surface is assumed to be constant. No reactants precipitate. The amount of reactant A and product B is dependent on stage 1, the drying of the support. It is assumed, that the reaction is first order with respect to A and that no concentration differences exist inside the impregnation solution.

The change in the concentration of A in the top layer is caused by reaction, which lowers the concentration, and drying, which increases the concentration. This gives

$$\frac{d[A]'_{tl}}{dt'} = -K_1[A]'_{tl}(t') + \frac{aW_{tl}}{V'_{tl}(t')}[A]'_{tl}(t) \quad (33)$$

where $[A]'_{tl}(t)$ is the concentration in the top layer (mol m^{-3}). The $'$ sign refers to the second period (drying of the top layer only). The first term on the right hand side gives the change due to reaction, the second term the change due to the volume decrease. The volume change can be described by

$$V'_{tl}(t') = V_{0,tl} - aW_{tl}t' = W_{tl}(L_1 - at') \quad (34)$$

in analogy with Equation 10. L_1 is the length of the top layer pore. Equation 33 can be rewritten, considering

$$C'_{A,tl}(\tau') = \frac{[A]'_{tl}(\tau')}{[A]_{0'}}[A]_{0'} = [A]_{sup}(\tau = 1)$$

$$\tau' = \frac{t'}{L_1/a} \quad (35)$$

It should be remembered, that the starting concentration, $[A]_{0'}$ comes from solving the first stage, the drying of the support. Substituting Equations 34 and 35 in Equation 33 yields

$$\frac{dC'_{A,tl}(\tau')}{d\tau'} = -\varphi' C'_{A,tl}(\tau') + \frac{C'_{A,tl}(\tau')}{(1 - \tau')}$$

$$\text{with } \varphi' \equiv \frac{L_1/a}{1/k_1} = \frac{k_1 L_1}{a} \quad (36)$$

Here φ' presents the ratio of the characteristic drying

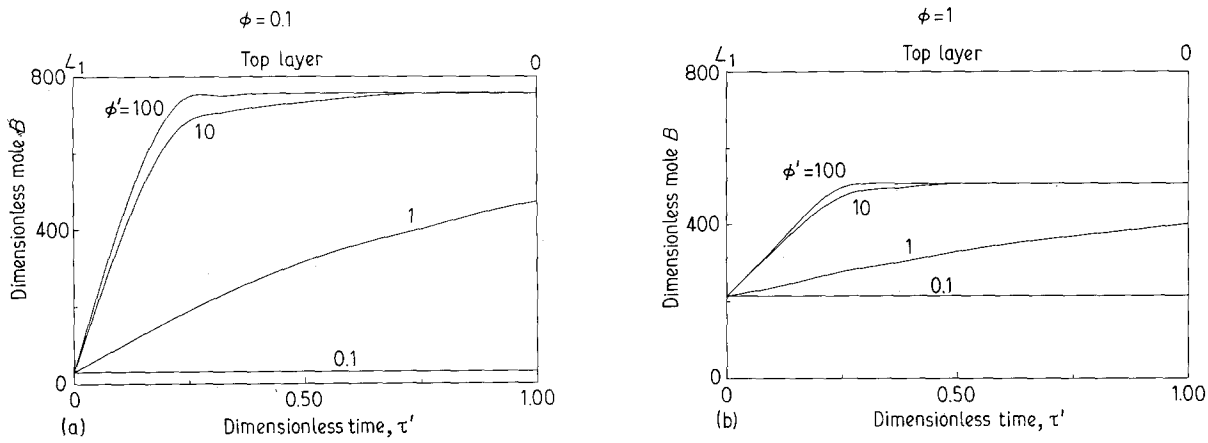

Figure 15 The amount of *B* deposited in the top layer pore relative to the initial amount of *A* present in the top layer pore as a function of the dimensionless time τ' for several φ and φ'.

time of the top layer to the characteristic reaction time. This is completely comparable to the parameter φ in the previous section. Solving Equation 36 with the boundary condition that $C'_{A,tl} = 1$ for $\tau' = 0$ finally results in

$$C'_{A,tl}(\tau') = \frac{1}{(1-\tau')} e^{-\varphi'\tau'} \qquad (37)$$

Equation 37 gives at any time, τ', the concentration of reactant *A* in the impregnation solution. It should be remembered, that $C'_{A,tl}$ is defined in relation to the concentration obtained after directly drying the support (at $\tau = 1$). The actual concentration of *A* in the top layer can therefore be very high.

The total amount of *B* produced is equal to

$$N'_{B,tl} = 1 - N'_{A,tl}(\tau') = 1 - e^{-\varphi'\tau'} \qquad (38)$$

This equation gives at any time the amount of *B* deposited, relative to the starting amount of *A* present in the top layer, after drying the support. It should also be considered, that an amount of *B* has already deposited in the top layer, directly after drying the support. The total amount of *B* deposited inside the top layer during the two periods of the process (drying of support and top layer) relative to the amount of *A* initially present in the top layer at time, τ', $N^{tot}_{B,tl}(\tau')$, is

$$N^{tot}_{B,tl}(\tau') = \frac{M^{tot}_{B,tl}(\tau')}{M_{A,0,tl}} = N_{A,tl}(\tau = 1)(1 - e^{-\varphi'\tau'}) + N_{B,tl}(\tau = 1) \qquad (39)$$

where $N_{A,tl}(\tau = 1)$ is given by Equation 30 and Fig. 11 and $N_{B,tl}$ is given by Equation 32 and Fig. 12. Fig. 15 presents the dimensionless amount of *B* with respect to the initial concentration of *A* in the top layer. It can be seen, that dependent on the value of the parameters φ and φ', a large increase in amount of *B* can be present in the pores of the top layer. At low φ, the highest relative amounts of *B* are deposited. The value of φ' will determine the deposit profile of *B*. That is, *B* will be deposited in a way, shown in Fig. 14, due to drying of the top layer pores. Therefore it is possible to create a profile of product *B* in the top layer pores.

At high φ and φ', the profile is almost flat and *B* is distributed homogeneously. This is because the reaction rate is high and most of the *A* present will be immediately converted. At high φ, most of the *B* will be deposited in the support. At low φ, but high φ', the *A* present in the top layer pores will be immediately converted to *B*. Loads can become very high in this case (Fig. 15). The deposition is homogeneously distributed.

At low φ' and φ, most *B* is deposited at the pore entrance. The low φ however means, that a part of *B* has homogeneously deposited in the top layer during the drying of the support. A very low φ and moderate φ' gives the most pronounced profile of *B* in the top layer (Fig. 15a, $\varphi = 0.1$ and $\varphi' = 1$). Thus it is possible to control the place of deposition by controlling φ and φ', which means control of the drying and reaction rates. These factors can be controlled independently, e.g. by temperature and humidity control.

Unfortunately the model above is far too simple to describe these profiles accurately. As stated before, the drying rate will be a function of the deposition rate and profile. Qualitatively it can be said, that at high deposition rates, the drying will become slower (smaller available drying surface) and the reaction faster (smaller volume and thus higher concentration of *A*). Therefore *B* will tend to deposit faster and thus more homogeneously. In view of this explanation it seems more difficult to obtain a deposition at the pore entrance only. A much more detailed analysis of the process should be conducted to verify this qualitative visualization however.

An additional complication is the precipitation of reactants due to the short drying time of the thin γ-alumina film. The thus formed solid state mixture will melt, decompose or react further [9], but the implications for the deposition profile of *B* are very difficult to describe.

4.2.3. Summary

In this section the consequences of drying the top layer only on the concentration of reactant *A* and product *B* were reviewed. It has been shown, that high loads of *B* inside the top layer are possible. It is

however very difficult to establish the exact profile of product B inside the pore of the top layer.

5. Comparison of model and experiments

Table V showed for silver a difference between drying and reaction occurring simultaneously or sequentially. For magnesia this difference did not exist (Table VI). If the support is dried first (at 40 °C) no reaction will occur. The reactants are forced to accumulate inside the top layer. This is comparable to a situation with a very low reaction rate in the proposed theory (low φ, see Fig. 11). The system is then heated to 90 °C and finally calcined. All the reactants are converted inside the top layer during this process. This gives very high loads inside the top layer, as demonstrated by Tables V and VI.

If simultaneous drying and reaction occur, the load inside the top layer will depend upon the ratio of the drying and reaction times, according to the model presented above. The drying constant for a supported thin film is of the order of $2 \times 10^{-8}\ m\,s^{-1}$ [13]. Kinetic observations showed a reaction constant of $6 \times 10^{-5}\ s^{-1}$ for the silver–urea reaction and a reaction constant of $5 \times 10^{-6}\ s^{-1}$ for the magnesium–urea reaction. Consequently $\varphi = 6$ for the silver–urea and $\varphi = 0.5$ for the magnesia–urea modification, according to Equation 16 with the thickness of the support equal to 2 mm.

A φ value of 6 means that the characteristic time of reaction is smaller than the characteristic time of drying (Equation 16). The reaction proceeds faster than the drying. The model predicts that, in this case, some silver will be deposited in the support (Fig. 10). This is experimentally verified by the EDX and SAM measurements on silver modified γ-alumina films and explains the poor loading of the top layer of sample 6 in Table V in comparison with the other samples of this table.

A φ value of 0.5 on the other hand means that the characteristic time of drying is smaller than the characteristic time of reaction. Drying proceeds faster than reaction. The model predicts a high accumulation of reaction products in the top layer in this case (Fig. 11). For the magnesia modification there should therefore be no difference in performing the drying and reaction step sequentially or simultaneously. This is experimentally verified by comparison of samples 1–4 and 2–5 in Table VI. The decrease in permeability is identical, irrespective of the modification procedure followed.

A large discrepancy however exists between samples 3 and 6 of Table VI. Obviously at high loads the different processing does have an effect. After two modification cycles 69% of the pore volume is already occupied by magnesia. This decrease of the pore volume will also diminish the drying surface area, resulting in an increased drying time. Consequently φ is increased and more magnesia will deposit in the support. Thus a maximum for the magnesia incorporation in the top layer is reached. Sample 6 in Table VI however is first dried. Reactants accumulate inside the top layer without reaction. As soon as the temperature is raised, reaction will occur, but mainly inside the top layer. This results in higher loads and a sharp decrease of the permeability compared to samples modified by simultaneous drying and reaction.

5. Conclusions

1. The reservoir method, employing the support as a reservoir for the impregnation solution, is suitable to obtain high loads in the top layer. The critical parameters are the drying time of the system in relation to the reaction time. If drying and reaction occur simultaneously, the drying rate should be faster than the reaction rate to obtain high loading of the top layer. Preferably the drying and reaction should be performed sequentially to be sure the impregnation solution is concentrated in the top layer prior to reaction. In this way a concentration up to 750 times the initial concentration of reactants can be realised inside the top layer.

2. The results obtained with the silver and magnesia modification on supported γ-alumina thin films could be satisfactorily described with the proposed theory for the reservoir method.

3. The highest load for silver was obtained by performing the drying and reaction step sequentially. In this way silver could be incorporated in the top layer up to about 67 wt %, corresponding to 70% of the initial pore volume. Above 50 wt % however the dispersion becomes worse, due to clustering. This is caused by the high mobility and poor wettability of silver on γ-alumina. Incorporation of more than 67 wt % silver introduces cracks in the thin γ-alumina film.

4. Magnesia could be incorporated in the top layer up to 45 wt %, corresponding to 85% of the pore volume, only if drying and reaction occurred sequentially. Although the permeability decreased sharply, only a slight pore size decrease was observed however, even at these high loads.

5. For γ-alumina the reservoir method seems to be only suitable to control the chemical nature of the surface, not to decrease the pore size. This is caused by the slit-shaped form of the pores in γ-alumina in combination with the distribution of the deposit inside the pore. At least 85% of the pore volume should be filled in order to decrease the pore size effectively. It can be expected however, that with other pore morphologies, a pore size decrease can be obtained with the reservoir method.

Acknowledgement

W. van Praag and M. Huis in 't Veld are gratefully thanked for performing some of the experiments. The preparation of the supports by L. Berkeveld of the N.K.A. is gratefully acknowledged. The research was made possible by financial assistance from the Innovative Research Program Committee on membranes.

References

1. R. J. R. UHLHORN, K. KEIZER and A. J. BURGGRAAF, *J. Mater. Sci.* **26** (1991) in press.

2. *Idem*, in "Advances in reverse osmosis and ultrafiltration", edited by T. Matsuura (ACS, Washington, 1989) p. 235.
3. *Idem*, Dutch Patent 8 901 080, (1989).
4. *Idem*, *J. Membr. Sci.* to be published.
5. *Idem*, *ibid.* to be published.
6. K. P. de JONG and A. W. GEUS, *Study Surf. Sci. Catal.* **16** (1983) 111.
7. R. J. R. UHLHORN, K. KEIZER and A. J. BURGGRAAF, *J. Membr. Sci.* **46** (1989) 225.
8. W. H. R. SHAW and J. J. BORDEAUX, *J. Amer. Chem. Soc.* **77** (1955) 4729.
9. R. C. WEAST (ed.) "Handbook of Chemistry", 67th Edn (CRC Press, Cleveland 1974) p. 6.
10. L. M. STRUBINGER, G. L. GEOFFROY and M. A. VANNICE, *J. Catal.* **96** (1985) 72.
11. D. BRIGGS and M. P. SEAH (eds) in "Practical surface analysis by auger and X-ray photoelectron spectroscopy" (J. Wiley & Sons, New York) 1983.
12. J. T. GRANT, *Appl. Surf. Sci.* **13** (1982) 35.
13. J. H. L. VONCKEN, private communication.

Received 1 October 1990
and accepted 18 March 1991